energies

MDPI

Article

Longwall Top-Coal Caving Mechanism and Cavability Optimization with Hydraulic Fracturing in Thick Coal Seam: A Case Study

Zhaohui Wang [1,2,*], Yuesong Tang [1] and Hao Gong [1]

[1] School of Energy and Mining Engineering, China University of Mining and Technology, Beijing 100083, China; BQT2000101016@student.cumtb.edu.cn (Y.T.); ZQT1900101006G@student.cumtb.edu.cn (H.G.)
[2] Coal Industry Engineering Research Center of Top-Coal Caving Mining, Beijing 100083, China
* Correspondence: zhwang1024@cumtb.edu.cn

Abstract: Longwall top-coal caving mechanisms and cavability optimization with hydraulic fracturing are analysed in this study. Based on the geological and geotechnical conditions of the Dongzhouyao coal mine, it is revealed that top-coal failure mechanisms are dominated by both compressive and tensile stresses. Ahead of the face line, shear failure initiates at the lower level of the top-coal and propagates to the upper level. Compressive stress-induced damage leads to obvious deterioration in tensile strength, causing the onset of tensile failure in the top-coal behind the face line. Accumulated plastic strain (APS) is selected as a top-coal cavability indicator. The cavability degrades gradually at the higher elevation of the top-coal while it is greatly strengthened as the top-coal approaches closer to the face line. In a thick coal seam without hydraulic fractures, the maximum APS occurs at the middle section of the face length in the Longwall top-coal caving (LTCC) panel. After hydraulic fracturing, top-coal cavability is significantly enhanced. But the spatial distribution of the APS transitions from uniform to non-uniform type due to the existence of hydraulic fractures, causing great variety in the cavability along the panel width. With increasing fracture intensity and fracture size, the failure zone expands significantly ahead of the longwall face, which means the cavability becomes increasingly favourable.

Keywords: longwall top-coal caving; failure mechanism; top-coal cavability; stress path; hydraulic fracturing

Citation: Wang, Z.; Tang, Y.; Gong, H. Longwall Top-Coal Caving Mechanism and Cavability Optimization with Hydraulic Fracturing in Thick Coal Seam: A Case Study. *Energies* **2021**, *14*, 4832. https://doi.org/10.3390/en14164832

Academic Editor: Mofazzal Hossain

Received: 5 July 2021
Accepted: 5 August 2021
Published: 8 August 2021

1. Introduction

Coal seams thicker than 3.5 m account for about 45% of the proven coal reserves and about 40% of the annual coal production in China [1]. Longwall top-coal caving (LTCC) is widely used for extracting such thick coal seams. That means the LTCC technique plays an important role in providing energy for the rapid social development of China. A typical layout of an LTCC face is presented in Figure 1, where a thick coal seam is divided into two sections. The lower section is sliced by a shearer installed along the floor line of the seam, transported by a face conveyor installed near the face wall. The upper section (top-coal) fails and caves behind the hydraulic support under the overburden pressure. There is a moveable flipper attached to the rear canopy of the support. By moving the flipper, a drawing window appears. Through the drawing window, loose top-coal is delivered to the rear face conveyor and transported in the same path as that delivered by the front face conveyor [2]. As shown in Figure 1, LTCC extraction is mainly comprised of two processes, including progressive fracturing of intact top-coal and subsequent drawing of loose top-coal. Top-coal thickness is generally at a 1 to 3 times lower cutting height, which means improving the top-coal recovery rate is of great importance in LTCC mining. The top-coal recovery rate is dependent on continuous caving and drawing behaviour

behind the support. Such behavior relies heavily on the fracturing of top-coal ahead of the longwall face. Since top-coal fails under the influence of overlaying strata movement, top-coal cavability is closely related to the conditions of the overlaying strata. Delayed caving and the formation of large blocks should be avoided in the top-coal, which may result in safety and production concerns of such coal mines.

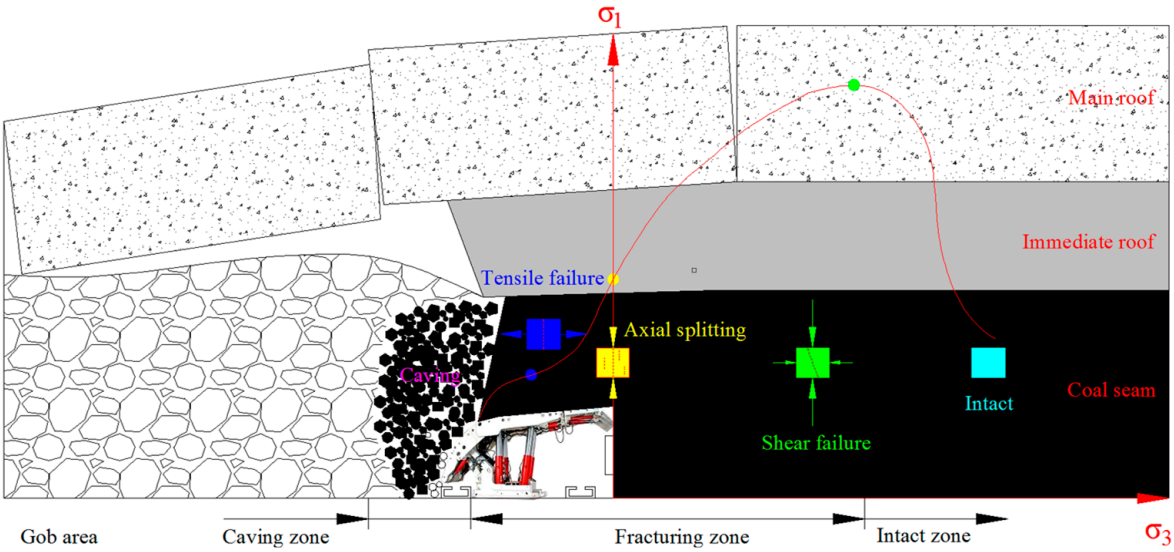

Figure 1. Layout of LTCC face.

It is commonly observed that the top-coal cannot cave in a timely manner (Figure 2a) or forms a large broken block (Figure 2b) behind the support. In this case, the top-coal is not able to flow onto the rear face conveyor through the drawing window; the drawing window may even be choked by the large block, causing a production halt of the longwall face. Such undesired caving behaviors cause many losses to the top-coal. The lost top-coal is left in the gob area, leading to a dramatic decrease in the recovery rate or even failure implementation of LTCC mining in thick coal seams [3]. As a result of such critical features, the recovery rate of LTCC panel in the thick coal seam is relatively low compared with that in conventional longwall panel with large mining height. Thus, before practical application to the thick coal seam, the top-coal cavability should be carefully assessed regarding LTCC technique. In order to realize the successful implementation of LTCC mining within thicker coal seams in China, top-coal failure mechanisms and accurate prediction of the caving behaviors are analyzed in this paper.

(**a**) (**b**)

Figure 2. Undesired caving behaviors of top-coal. (**a**) Delayed caving; (**b**) formation of the large top-coal block.

Understanding failure mechanisms of the top-coal is the first stage in designing an efficient LTCC panel. Therefore, many theoretical and experimental works have been done for achieving a deeper understanding of top-coal failure mechanisms in thick coal seams [4–6]. Similar to mechanical responses of the surrounding rock during tunnel excavation, LTCC extraction involves several failure mechanisms as shown in Figure 1, including gravity driven failure (tensile failure) at the cave boundary, axial splitting due to stress relaxation in the vicinity of the longwall face, and shear failure arising from abutment loading ahead of the face line. Despite different research priorities, a consensus has been reached in previous studies that the following issues significantly influence the top-coal failure process: coal strength characteristics, mining induced stresses, cutting height, top-coal thickness, and roof conditions. Successful characterization and accurate prediction of top-coal cavability is another prerequisite in LTCC panel design. The cavability refers to the capability of intact top-coal to unravel under the influence of coal seam extraction. In order to assess the adaptability of LTCC mining to various geological conditions, top-coal cavability prediction methods have been evaluated by using theoretical and numerical methods [7]. At the heart of these predictions is the ability to identify the right failure mechanisms of the top-coal. An extensively used caving factor (CF), proposed by Alehossein et al., is based on the assumption that shear failure of the top-coal initiates ahead of the longwall face and tension failure subsequently occurs at the rear of the face line [8]. According to the value of CF, caving performance of LTCC is qualitatively classified into four types, including excellent (0.9–1), good (0.8–0.9), medium (0.7–0.8), and poor (<0.7). Though a theoretical method is convenient in practical applications, the result is achieved based on a series of assumptions, and sometimes, a set of case histories of LTCC mining are necessary, making it a semi-empirical criterion. Besides, due to the rapid development of computer technology, numerical modeling is increasingly used in investigating the performance of LTCC mining. Based on properly validated numerical models, fracturing and caving processes of the top-coal can be accurately reproduced [4]. The plastic zone, the degree of plastic deformation, and mining-induced fracture development in the top-coal are commonly applied to the characterization and prediction of the cavability in LTCC mining operations.

There are lots of fractures existing in thick coal seams. Many researchers have been aware that fracture distribution leads to great differences in top-coal recovery rate in LTCC practices. That means pre-existing fractures may play a key role in the failure process of the top-coal. Therefore, it is necessary to take the influences of fracture distribution into account in evaluating top-coal cavability. Wang et al. tried to predict the size distribution of top-coal fragmentation by building a discrete fracture network according to fracture distribution in thick coal seams [9]. Xie et al. analyzed fractal characterization of mining induced fractures and found a strong correlation between fracture distribution and top-coal cavability [10]. Jin et al. compared fracture distribution and top-coal recovery rate in various thick coal seams [11]; after that, a caving index table was established based on the development degree of pre-existing fractures in coal seams. The influence of fracture orientation on top-coal recovery rate is studied by Wang et al. using physical modeling methods [12]. With the increasing angle between the face advance direction and dip direction of the pre-existing fractures, the top-coal recovery shows a decreasing trend in the LTCC panel.

Up to now, the LTCC mining method has been successfully applied in thick coal seams with various conditions, such as steeply inclined thick coal seams and ultra-thick coal seams [13–15]. Though the method has been operating effectively in China for many years, accurate prediction and assessment of top-coal cavability for LTCC operations remain problematic due to a poor understanding of top-coal caving mechanisms. Therefore, the main objective of this study is to explore failure mechanisms of the top-coal in a thick coal seam and cavability improvement induced by hydraulic fracturing. In the next section, a case study in Dongzhouyao coal mine is provided and analyzed. In Section 3, a numerical model for LTCC mining is developed, and failure mechanisms of top-coal are analyzed based on stress distribution in the top-coal. Five numerical models with random-distributed fractures are properly established, and the influences provided by hydraulic fractures on

the cavability are analyzed in Section 4. Lastly, the main conclusions of the research are presented in Section 5.

2. LTCC Performance at the Study Site

2.1. Longwall Mining Conditions

Dongzhouyao coal mine is located in Datong City, Shanxi Province, China. All panels in this underground mine use the LTCC method to extract a thick coal seam, which is nearly horizontal with a dip angle smaller than six degrees. The cover depth and average thickness of the coal seam are 350 m and 8 m, respectively. The target panel for this case study is panel 8202 as shown in Figure 3. The longwall panel is 110 m wide along the dip and 1200 m long in the strike direction. The cutting height and top-coal thickness are 3 m and 5 m, respectively. Both main and tail gates are driven along the floor of the thick coal seam. Based on core logging, a typical geological column of the study site was constructed and is presented in Figure 4. The roof strata belongs to mediate-hard type in the target longwall panel. There are mainly three kinds of rocks, including the mudstone, siltstone and sandstone. According to the engineers, a layer of sandstone with a thickness of 6.3 m serves as the main roof. An in situ rock stress measurement was carried out three times at the mine site with the overcoring relief method [16]. The observation locations are shown in Figure 3. By ignoring the tectonic stress, the results indicate that the major principal stress, in a vertical direction, is 10 MPa. Both intermediate and minor principal stresses are in horizontal directions. The magnitudes are about 6.2 MPa and 3.3 MPa, respectively.

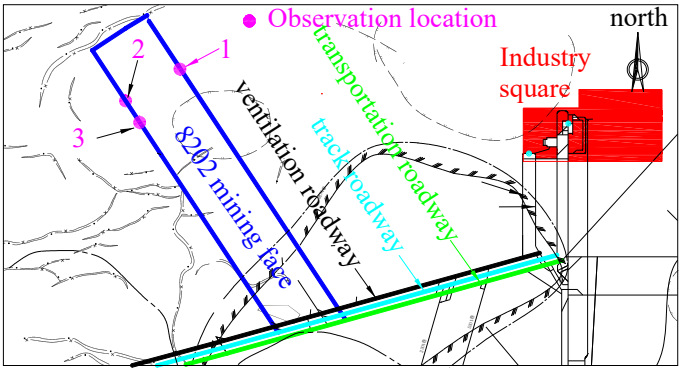

Figure 3. Plan view of panel 8202 layout.

2.2. Material Properties of the Rock

In order to determine the rock properties at Dongzhouyao coal mine, standard cylindrical specimens of the related rocks were prepared as shown in Figure 5a. Uniaxial compression tests were conducted on these specimens. Failure modes of different rocks are presented in Figure 5b, which indicates axial splitting occurs on the coal specimen while the mudstone and sandstone specimens fail in shear.

Stress–strain curves of three kinds of rock specimens are presented in Figure 6, where axial compression strain appears as a positive number, while extension strain appears as a negative number. Figure 6 indicates uniaxial compressive strength (UCS) of the coal, mudstone and sandstone are 19 MPa, 46 MPa, and 80 MPa. Stress and strain values at points A, B, and C are used to determine elastic modulus and Poisson ratio because the radial strain is small, and no macro-cracks appear in the specimen at the deformation states. Critical experimental data are listed in Table 1, where ε_r, ε_a, and σ represent radial extension strain, axial compression strain, and axial stress value at points A, B, and C. Then, the Poisson ratio (ν) and elastic modulus (E) of the coal, mudstone, and sandstone are determined. The tensile strength (σ_t) obtained from the splitting tests are also listed in Table 1.

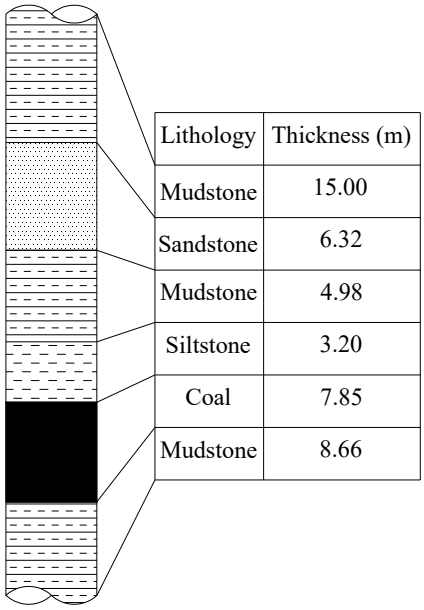

Lithology	Thickness (m)
Mudstone	15.00
Sandstone	6.32
Mudstone	4.98
Siltstone	3.20
Coal	7.85
Mudstone	8.66

Figure 4. Geological column.

(**a**) (**b**)

Figure 5. Rock specimens before and after uniaxial compression test. (**a**) Intact specimens; (**b**) failure modes.

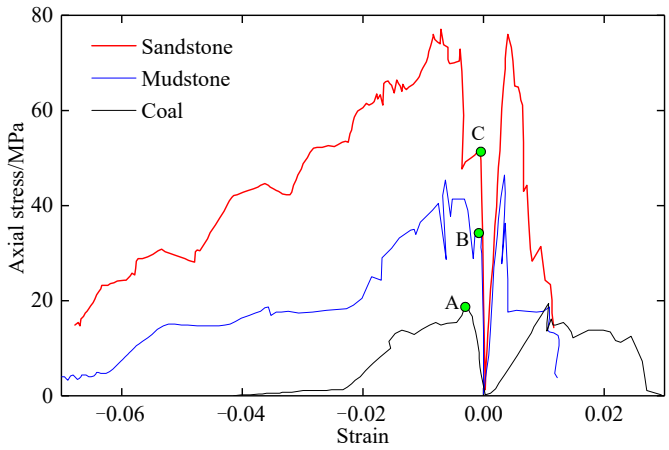

Figure 6. Stress–strain curve of rock specimens.

Table 1. Experimental result of unconfined compression tests.

Rock Type	ε_r (%)	ε_a (%)	ν	σ (MPa)	E (GPa)	UCS (MPa)	σ_t (MPa)
Coal	0.35	1.1	0.32	19	1.7	19	1.3
Mudstone	0.06	0.2	0.30	31.48	15.4	46	3.8
Sandstone	0.06	0.25	0.24	52.0	20.5	80	6.0

2.3. Field Measurement

The borehole camera detection technique is commonly used to observe fracture development in the top-coal. Accordingly, borehole camera detection was conducted in the Dongzhouyao coal mine. Borehole camera detection provides quantitative data to assess top-coal failure mechanisms and examine the performance of LTCC operations. After drilling of the borehole in the top-coal, mining-induced fractures that intersect with the borehole wall can be detected directly with the borehole camera. Two vertical boreholes were drilled in the roof of the main gate of panel 8202. Borehole A located 10 m ahead of the longwall face and borehole B was drilled at the rear of the face line. Then, the failure characteristics of the top-coal were measured and saved as a video file. The results are plotted in Figure 7, which revealed the top-coal at different levels in the vertical direction showed great differences in failure degree. Fracture development of the top-coal at the lower level was sufficient, while it was insufficient at the higher level. Top-coal cavability is positively related to fracture development. Therefore, top-coal cavability at the lower level is better than that at the higher level. Mining-induced fractures of top-coal are closed ahead of the longwall face. These closed fractures open gradually in the vicinity of the longwall face. Closed fracture indicates top-coal fails in shear, while open fracture indicates top-coal fails in tension. Thus, it can be concluded that, in LTCC mining, top-coal undergoes two failure processes, including shear failure ahead of the longwall face and tensile failure at the rear of the face line. This conclusion is consistent with top-coal failure patterns shown in Figure 1. Based on borehole camera detection, it is found mining-induced fractures at the upper level of top-coal are not fully developed at the rear of the face line. Therefore, top-coal recovery at Dongzhouyao mine is about 75%, less than the average value of LTCC faces in China. Based on the conclusions of a project undertaken by the authors, hydraulic fracturing was latterly carried out at this mine to strengthen top-coal cavability.

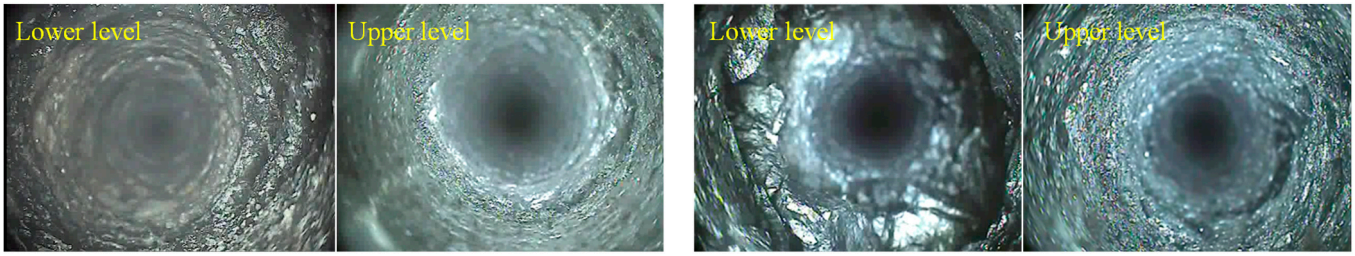

Figure 7. Borehole camera detection. (**a**) Borehole A; (**b**) Borehole B.

3. Numerical Analysis of Top-Coal Failure Process

3.1. Model Configuration

Non-linear numerical analysis was carried out with FLAC 3D software in this section. This software is based on a finite difference approach and is extensively used globally for mining applications [17]. The numerical model size built for this study was 200 m × 200 m × 120 m in x-, y- and z-axes (Figure 8). Two sides and the bottom of the model have fixed displacement boundaries, while vertical stress with the value of 7 MPa was applied on the top surface to simulate the gravity of overlaying strata, which were not included in the numerical model. According to the true situation in the mine under consideration, in situ stresses were applied in the form of initial stress with the horizontal to vertical stress ratio set to 0.6 and 0.3, respectively, in the x- and y-directions. In the coal seam, the panel width was 100 m in dip direction and advances in accordance with y-direction.

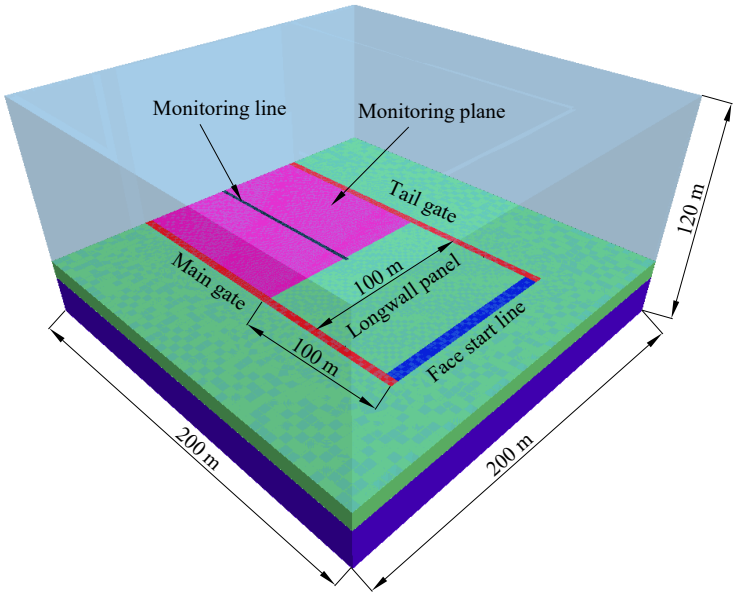

Figure 8. Numerical model layout.

The strain-softening constitutive model and Mohr–Coulomb failure criterion were used for simulating mechanical behaviors of the rocks induced by LTCC operations. Based on intact rock properties obtained from a laboratory test, rock mass properties for the numerical simulation, as listed in Table 2, were determined by using the GSI system proposed by Brown et al. [18]. Note m, k, and n were unknown parameters of the softening model developed by Wang et al. [19–21].

Table 2. Properties for numerical simulation.

Properties		Coal	Mudstone	Siltstone	Sandstone
Bulk modulus (GPa)		1.8	3.6	7.2	9.6
Shear modulus (GPa)		0.6	1.6	4	6.6
Internal cohesion (MPa)		2	4	6	10
Friction angle (deg.)		30	33	37	42
Tensile strength (MPa)		0.6	1	1.5	3
Dilation angle (deg.)		20	10	10	10
Softening parameters	m	0.003	0.0025	0.002	0.001
	k	1.3	0.59	0.63	0.40
	n	300	320	380	600

After excavation, the stress recovery phenomenon would occur in the gob area due to the continuous consolidation of caving materials. Accordingly, the gob area was simulated with a double-yield criterion, which was effective in modeling the consolidation behaviour of the caving materials. The gob material was changed into a double-yield model at 5 m behind the longwall face. The gob width was equal to the face length. The authors have established a function for controlling the evolution of the cap pressure composed of the double yield model, which is expressed as Equation (1) [19]. Material properties of the gob area were determined by comparing the modeling result with that predicted by Slamon's empirical model, which is listed in Table 3 [19].

$$p = a\left(e^{b\varepsilon_m^{ps}} - 1\right) + c\varepsilon_m^{ps} \quad (1)$$

Table 3. Gob Material Properties.

Property	Bulk Modulus (GPa)	Shear Modulus (GPa)	Cohesion (MPa)	Friction (°)	Tension (MPa)	a (MPa)	b	c (MPa)
Value	1.2	0.6	0	30	0	60	15	20

Note p is the cap pressure, ${\varepsilon_m}^{ps}$ is the volumetric plastic strain of caved materials, and a, b, and c are the cap pressure model parameters in Equation (1).

In this numerical analysis, the solution stages consisted of the excavation of main and tail gates and the continuous advance of the longwall panel. As the longwall face advancement reached 100 m, modeling results were extracted from the numerical model. That meant that the data analysed in this study were achieved when the distance between the longwall face and face start line increased to 100 m. In order to extract numerical data, monitoring line and plane were installed in the numerical model as shown in Figure 8. The zone covered by the monitoring plane was the focus area in the current study. Note that the location of both the monitoring line and monitoring plane were 8 m above the floor of the thick coal seam.

3.2. Model Validation

Three monitoring stations were installed in the main gate. The distance from the longwall face to the first station was 50 m and the horizontal interval between different stations was 30 m. One stress meter was embedded in the seam at each station through which mining-induced abutment stress in the coal seam was measured and recorded. Deformation of the main gate was drastically strengthened by the longwall mining at about 20 m in front of the face line. Thus, two rows of hydraulic columns were installed to strengthen surrounding rock stability within this scope, which is common as a pre-supporting region of the main gate. The evolution of the supporting resistance within the pre-supporting region was recorded at the same time. Measured data were compared with vertical stress distribution obtained from the numerical model in Figure 9. In situ observed vertical stress agreed well with the numerical result. Both in situ measured and predicted data showed that, under the influence of LTCC mining, vertical stress of the coal seam started to increase at 30 m ahead of the longwall face. As the distance between the top-coal and face line decreased to 7.5 m, the vertical stress reached a maximum value, 19 MPa, which was 1.9 times the initial magnitude. That meant the shear failure in the thick coal seam initiated at this location. After that, the top-coal showed strain softening behavior and the bearing capacity began to deteriorate, so that the vertical stress presented a downward trend after the peak point. Though the unit of the support resistance (kN) in the pre-supporting area is not consistent with that of the vertical stress (MPa), it presented a similar evolving tendency with the abutment stress. Good consistency between the field-observed and model-predicted data demonstrated that the numerical model could simulate top-coal caving behaviour with good accuracy.

3.3. Top-Coal Failure Mechanisms

3.3.1. Failure Zone of the Top-Coal

The failure state of the top-coal at 100 m of face advance is displayed in Figure 10. As can be seen from the Figure, the failure of top-coal develops upward of the top surface of the thick coal seam in a vertical direction. In the horizontal direction, top-coal failure zone extends maximally to 8 m inward the face line. The expansion range decreases from 8 m at the lower level to 3 m at the upper level of the top-coal. That implied a failure degree of top-coal decreases with growth in the vertical level, which was consistent with fracture development in the top-coal detected with the borehole camera. The top-coal failed in both tension and shear. In the top-coal ahead of the longwall face, shear failure occurs firstly while, at the rear of the face line, tensile failure appears subsequently. Therefore, mining-induced fractures detected in front of the face line were closed, and these fractures opened

gradually in the vicinity of the face line. The model result, therefore, agreed well with the field measurement. In LTCC mining, the top-coal experienced two failure processes, namely, shear failure and tensile failure, which was divided by the face line.

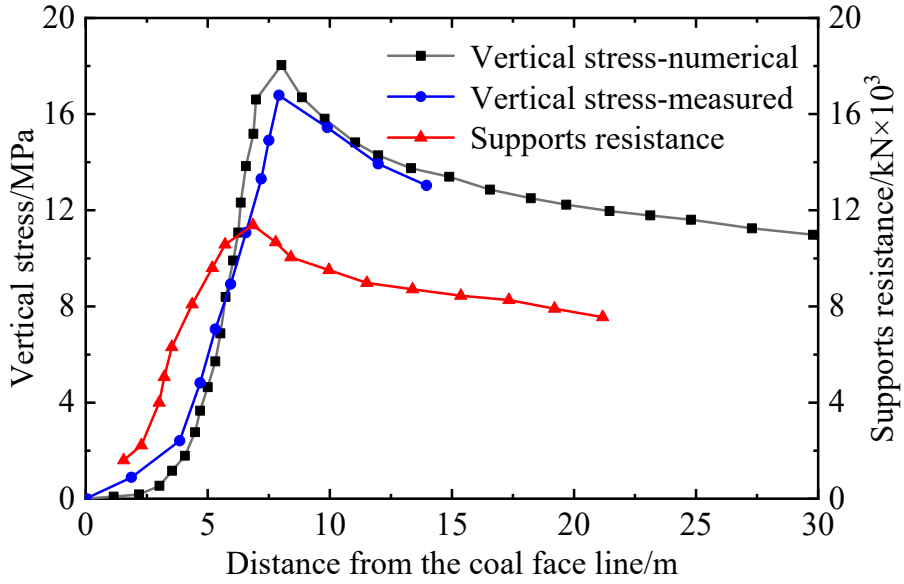

Figure 9. Comparison of vertical stress between measured data and numerical results.

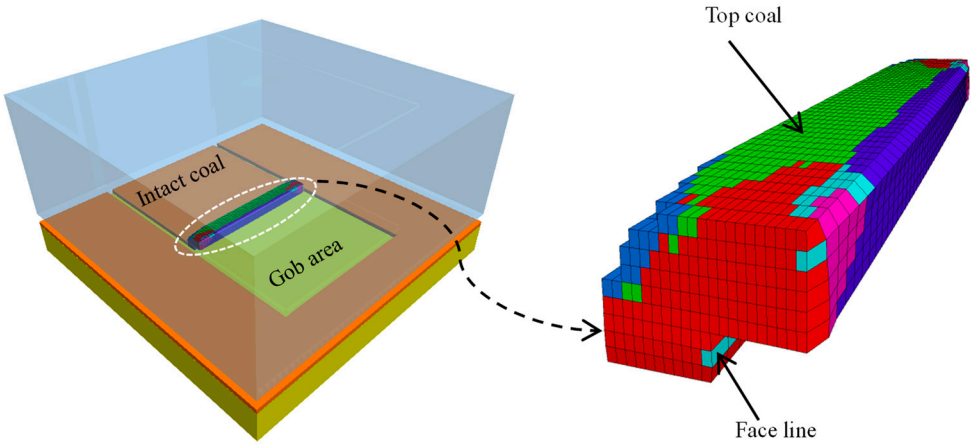

Figure 10. Failure zone of top-coal at 100 m of face advance.

3.3.2. Distribution of Principal Stresses

According to the Mohr–Coulomb failure criterion used in this numerical study, the failure modes of top-coal can be explained by principal stress distribution. After 100 m of face advancement, the spatial distribution of the major and minor principal stresses on the monitoring plane is presented in Figure 11. Note that before the model extraction, the vertical stress and horizontal stress in advancing direction denote the major and minor principal stresses, respectively. According to Figure 11, the principal stresses are significantly influenced by mining operations. As the coal seam is mined out, the exposed roof strata will subside and cave. Under the influence of roof strata movement, the major and minor principal stresses start to increase at the distances of 30 m and 50 m in front of the longwall face, respectively. Further into the unmined coal seam, the principal stresses are not affected by the longwall mining. At the location of 8 m and 10 m ahead of the face line, the major and minor principal stresses reach the maximum points, respectively. The peak value is about 23 MPa for the former and 7.5 MPa for the latter. After that, both major and minor principal stresses drop drastically. The initial failure position of

top-coal in Figure 10 is consistent with the peak point position of major principal stress. This means that the shear failure starts to occur after the compressive strength has been reached by mining-induced stress. In the plastic zone, the top-coal shows strain-softening behavior, leading to a continuous decrease of the major principal stresses. At the rear of the face line, the major principal stress decreases to a residual value while the minor principal stress becomes negative, indicating the transition from compressive to tensile stress. Correspondingly, the top-coal failure mode changes from shear to tension, as shown in Figure 10. In addition, the stress magnitude on the two sides is obviously smaller than that in the central area of the longwall face. The width of the edge area with small stress reaches about 20 m, which may lead to undesirable cavability.

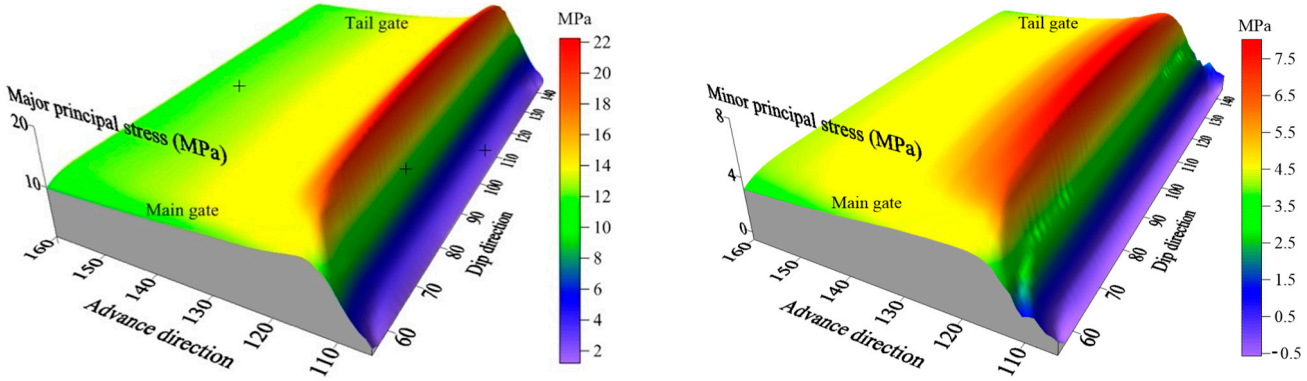

Figure 11. Spatial distribution of the principal stresses on the measuring plane.

The two-dimensional distribution of the principal stresses along the monitoring line is displayed in Figure 12, where a positive number on the horizontal axis means top-coal locates ahead of the face line while a negative number means at the rear of the face line. Peak values of the major and minor principal stresses, appearing in front of the longwall panel, are 23 MPa and 7.5 MPa, respectively, corresponding to 2.3 and 2.5 times the pre-mining stress. The peak location of the former is 2 m closer to the longwall face than that of the latter. After the minor principal stress has arrived at the peak location, its magnitude drops drastically because of the coal seam extraction. Decrease of the minor principal stress results in fast deterioration in the compressive strength of the top-coal. Strength loss leads to strain-softening behaviour of the top-coal, which means shear fail occurs at this deformation stage. At the face line, the minor principal stress decreases to zero. Top-coal stays in a biaxial compressive state. In this situation, top-coal tends to fail in spitting mode, as shown in Figure 5b. Such failure scenario is commonly observed at the side rib of the gate road, which also stays in a biaxial stress environment. As shown in Figure 12, the minor principal stress is loaded reversely at the rear of the face line. The negative value means it becomes tensile stress. After the shear failure stage in front of the longwall face, shear-induced damage is accumulated in the top-coal. The increasing damage causes obvious degradation in tensile strength. Therefore, tensile failure appears in the top-coal under small tensile stress behind the face line.

According to the comparison of Figures 10 and 12, it can be concluded that within the region of 8 m to 10 m inward the face line, the increase in the major principal stress and the decrease in the minor principal stress causes the appearance of large deviatoric stress in the top-coal. At the peak point of the major principal stress, the deviatoric stress is so large that shear failure occurs. After that, a continuous decrease in the minor principal stress leads to a decrease in the compressive strength of the top-coal. Thus, shear failure is experienced by the top-coal until the face line is reached. At the face line, the transition from compressive to the tensile stress of the minor principal stress leads to the transition from shear to tension of the failure pattern. That means failure patterns of the top-coal are mainly dominated by variation of the minor principal stress. Ahead of the face line, its

decrease causes the onset of shear failure. At the rear of the face line, its transition from compressive to tensile state causes the onset of tensile failure.

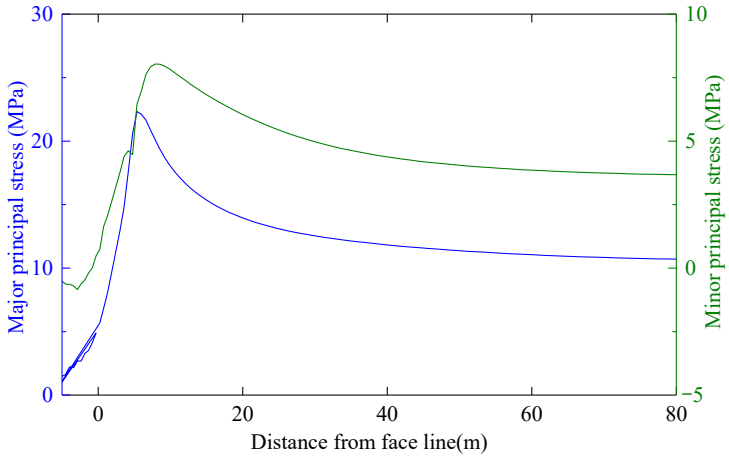

Figure 12. Distribution of the principal stresses along the measuring line.

3.3.3. Influence Provided by the Main Roof

With continuous face advancement, the immediate roof caves in a timely manner behind the longwall face. But a hanging phenomenon can occur to the main roof, forming a cantilever structure. The periodic rupture of the hanging main roof results in roof weighting in the longwall face. The hanging and fracturing behaviors of the main roof also cause many influences to the top-coal failure process [22]. As shown in Figure 13a, the main roof fractures when the face advancement increases to 90 m. Then, further advance of the longwall face leads to the increase in the hanging length of the main roof. After another 20 m of face advancement, the cantilever hanging behind the longwall face also reaches 20 m, which is plotted in Figure 13b. In this process, the evolution of the abutment stress with face advancement would occur. Though the failure width of the top-coal remains stable, the peak stress shows an increasing trend. When the cantilever length is small in Figure 13a, the largest stress is 18 MPa. This magnitude increases to 19.8 MPa as the hanging length of the cantilever rises to 20 m in Figure 13b. That means the failure degree of the top-coal would be improved and hence the cavability.

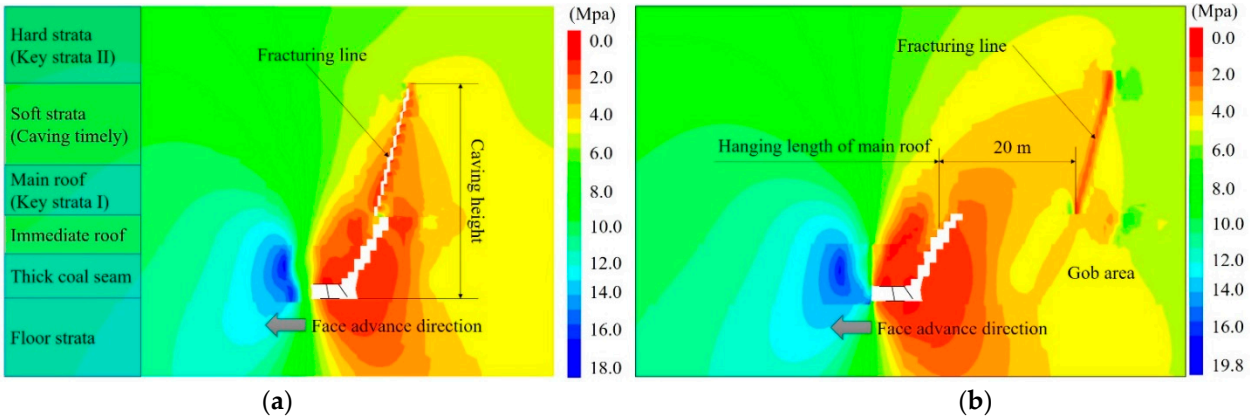

(**a**) (**b**)

Figure 13. The influence of roof hanging length on abutment stress distribution. (**a**) periodic rupture of the main roof; (**b**) the limit hanging length of the main roof.

The value of 20 m is the limit hanging length of the cantilever formed by the main roof. Thus, roof rupture appears when the longwall face advances 110 m from the face start line. A large-scale rupture of the main roof results in the sudden release of the strain

energy stored in the main roof. As shown in Figure 14, strain energy concentration in the main roof is obvious. The largest strain energy density reaches 33 J/m^3 before rupture. After fracturing of the main roof, the largest strain energy density decreases to 29 J/m^3. Besides, the strain energy concentration area shrinks due to roof rupture. The lost energy is divided into two parts. One section is consumed in the development of the rupture fracture within the main roof. The left is released and transmitted into kinetic energy of the broken block. The block impacts the bottom of the top-coal, which effectively promotes fracture development in the top-coal. Thus, both hanging and fracturing behaviors of the main roof helps to improve top-coal cavability and recovery rate.

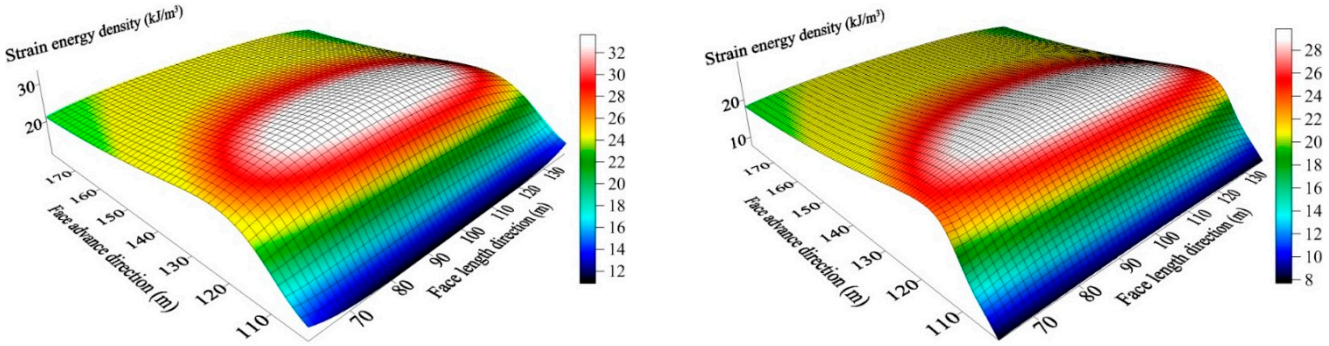

(**a**) (**b**)

Figure 14. Spatial distribution of the strain energy in the main roof. (**a**) before roof rupture; (**b**) after roof rupture.

3.4. Top-Coal Cavability Indicator

In previous research, top-coal cavability was assessed according to the scale of the failure zone, as shown in Figure 10. However, the area of the failure zone could not quantitatively indicate the failure degree (fracture development) of the top-coal; thus, this parameter is just a qualitative cavability indicator. According to laboratory tests, fracture development of rock specimens increases with the growth of accumulated plastic strain (APS), which is determined by Formula (2). Therefore, APS is taken as a top-coal cavability indicator in the presented study.

$$\Delta\varepsilon^{ps} = \sqrt{\frac{1}{2}\left(\Delta\varepsilon_1^{ps} - \Delta\varepsilon_v^{ps}\right)^2 + \frac{1}{2}\left(\Delta\varepsilon_v^{ps}\right)^2 + \frac{1}{2}\left(\Delta\varepsilon_3^{ps} - \Delta\varepsilon_v^{ps}\right)^2} \quad (2)$$

where $\Delta\varepsilon^{ps}$ indicates the APS, $\Delta\varepsilon_v{}^{ps} = (\Delta\varepsilon_1{}^{ps} + \Delta\varepsilon_3{}^{ps})/3$; $\Delta\varepsilon_i{}^{ps}$ means the principal plastic shear strain increment, where i = 1 or 3.

The APS distribution on the monitoring plane is presented in Figure 15. In the elastic area far away from the longwall face, there is no APS occurring in the top-coal, which means the top-coal stays intact. After the onset of the plastic failure at the peak point of the major principal stress, the APS of the top-coal increases continuously with decreasing distance from the face line. That means the cavability is improved as the top-coal approaches closer to the longwall face. Along the dip direction, the maximum value of the APS occurs around the middle section of the panel width. Under the current geological and geotechnical conditions, the maximum APS of top-coal increases to 0.12% in the vicinity of the face line. According to the stress–strain and failure mode of coal specimen obtained from the uniaxial compression test, fracture development of the coal is relatively low even though the APS reaches 0.12%. That means top-coal cavability in the Dongzhouyao coal mine is unsatisfactory. The average top-coal recovery rate is about 75%, according to mining engineers of the coal mine, relatively lower than the average value of LTCC mining. The predicted cavability indicator agrees well with the actual recovery of the top-coal. Besides, Figure 9 indicates the predicted stress shows a similar evolution trend with in situ measured data. That means the developed model is in good accordance with the actual situation

of the field practice. In China, the LTCC operation is considered successful with a seam thickness recovery rate larger than 85%. Thus, the unfavorable top-coal cavability needs to be enhanced to make the LTCC mining at Dongzhouyao mine becomes in line with national policy. Accordingly, hydraulic fracturing was carried out at this mine to decrease the loss of underground coal resources.

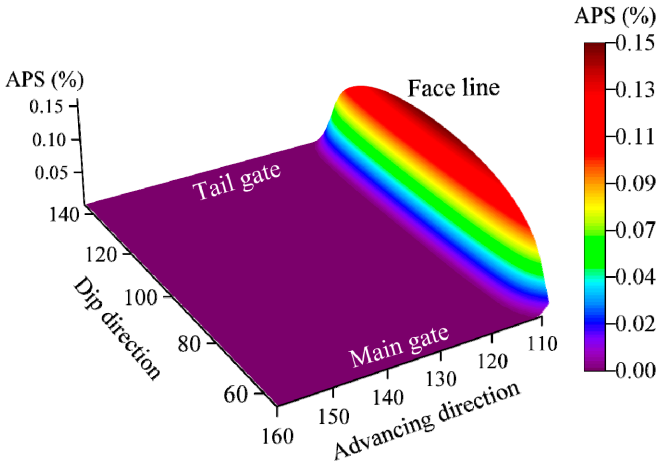

Figure 15. Distribution of APS on the measuring plane.

4. Influences of Hydraulic Fracturing on Top-Coal Cavability

4.1. Matrix of Models Analyzed

Hydraulic fracturing produces lots of hydraulic fractures in the top-coal, which plays a key role in optimizing the cavability. In order to evaluate the effectiveness of the hydraulic fracturing technique, sensitivity analysis is performed to understand the influence of hydraulic fractures on top-coal cavability. Initial conditions of the numerical models used in this Section are consistent with those built in Section 3 except that randomly distributed fractures are included in the study area. As shown in Figure 16, there are many hydraulic fractures existing in the newly developed model. In order to save the solution time, only the hydraulic fractures within the study area in concern were considered. Six modeling schemes were designed, which are listed in Table 4. Note the models utilized in schemes II and V have the same fracture parameters. In models I–III, the numbers of hydraulic fractures taken into account are 500, 2000, and 4000, respectively, used to assess the influence of fracture intensity on top-coal cavability. Models IV, V, and VI, with average fracture lengths of 1.2, 1.5, and 1.8 m, respectively, are utilized to investigate the influence of fracture size on top-coal cavability. All fractures included in the numerical models are built with the DFN method embedded in FLAC3D. In this paper, fracture positions are defined by a uniform distribution, dip angles by an exponential distribution, dip directions by a normal distribution, and fracture sizes (disk diameter) by a lognormal distribution. Strength parameters of the zones intersected with the hydraulic fractures in the study area are reduced by 50% of the value listed in Table 2.

Table 4. The designed modeling schemes.

Modelling Scheme	Model I	Model II	Model III	Model IV	Model V	Model VI
Fracture number	500	2000	4000	2000	2000	2000
Fracture size (m)	1.5	1.5	1.5	1.2	1.5	1.8

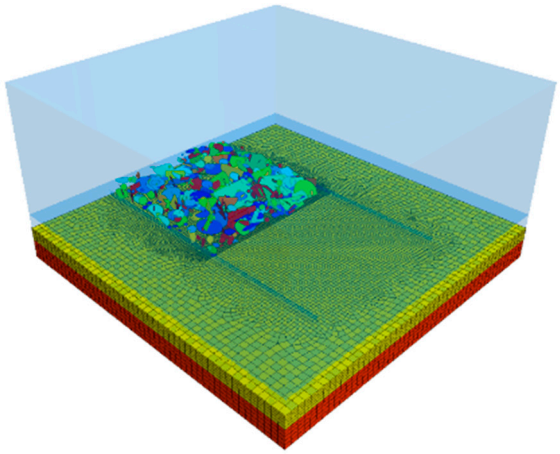

Figure 16. Numerical model with hydraulic fractures.

4.2. Influence on Failure Zone of Top-Coal

The influence of hydraulic fractures on failure zone extension of the top-coal is presented in Figure 17. An increase in fracture intensity and fracture length results in expansion of the failure zone ahead of the longwall face. The initial failure position of the top-coal moves further away from the face line. The failure zone extends from 12 m to 19 m as the number of fractures increases from 500 to 2000. The expansion increases from 13 m to 24 m ahead of the longwall face as the fracture size grows from 1.2 m to 1.8 m. Expansion of the failure zone enlarges the shearing process experienced by the top-coal. As a result, the tensile strength of the top-coal drops to a smaller value in the vicinity of the face line. Correspondingly, the range of tensile failure zone shows an expanding trend, as shown in Figure 17. Besides, the failure process of the top-coal initiates from the lower level of top-coal and propagates gradually towards the upper level.

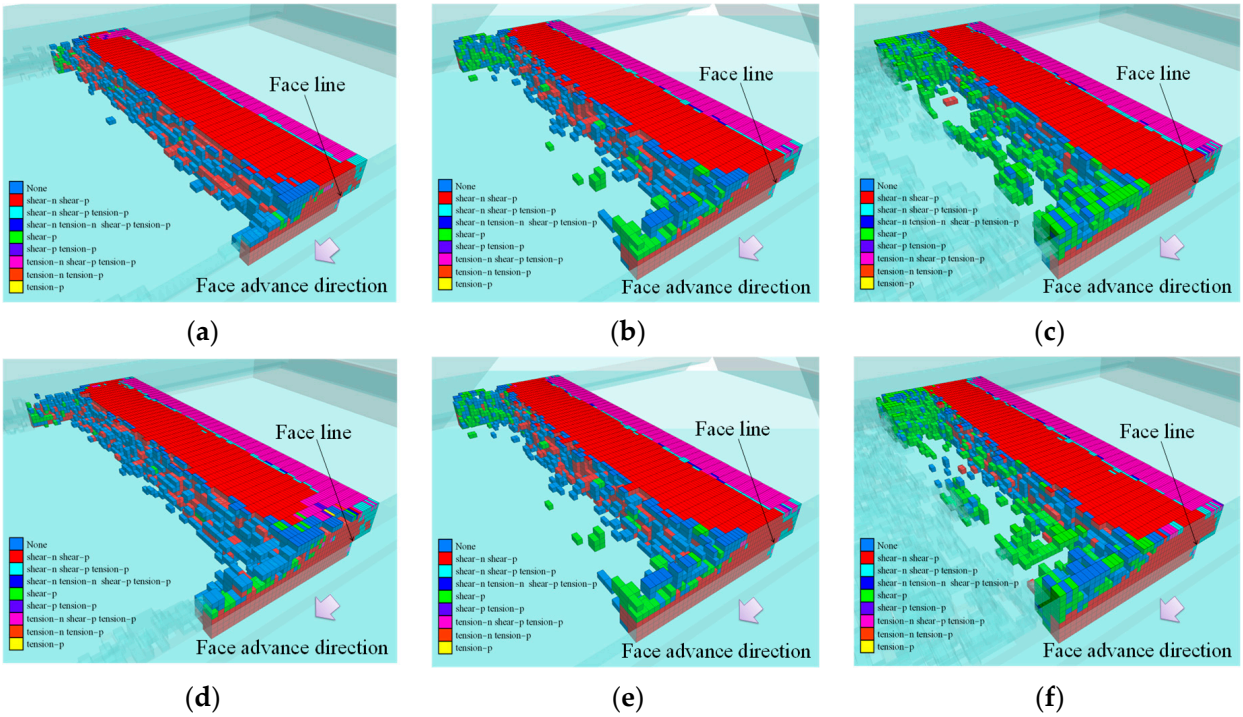

Figure 17. Influence of hydraulic fractures on failure zone of top-coal. (**a**) Model I; (**b**) Model II; (**c**) Model III; (**d**) Model IV; (**e**) Model V; (**f**) Model VI.

4.3. Influence on APS Distribution of Top-Coal

Distribution of the APS on the monitoring plane from models I to VI is plotted in Figure 18. Comparing Figure 18 with Figure 15, the hydraulic fractures cause an obvious increase in the APS. Also, its distribution along the dip direction of the longwall face transits from uniform to non-uniform type. That means top-coal cavability is non-uniform in thick coal seams with hydraulic fractures, causing great difficulty in its assessment. Such non-uniform distribution of the cavability indicator is brought up by the random distribution of hydraulic fractures. Besides, if the coal seam dips, the cavability indicator may also show asymmetrical mode.

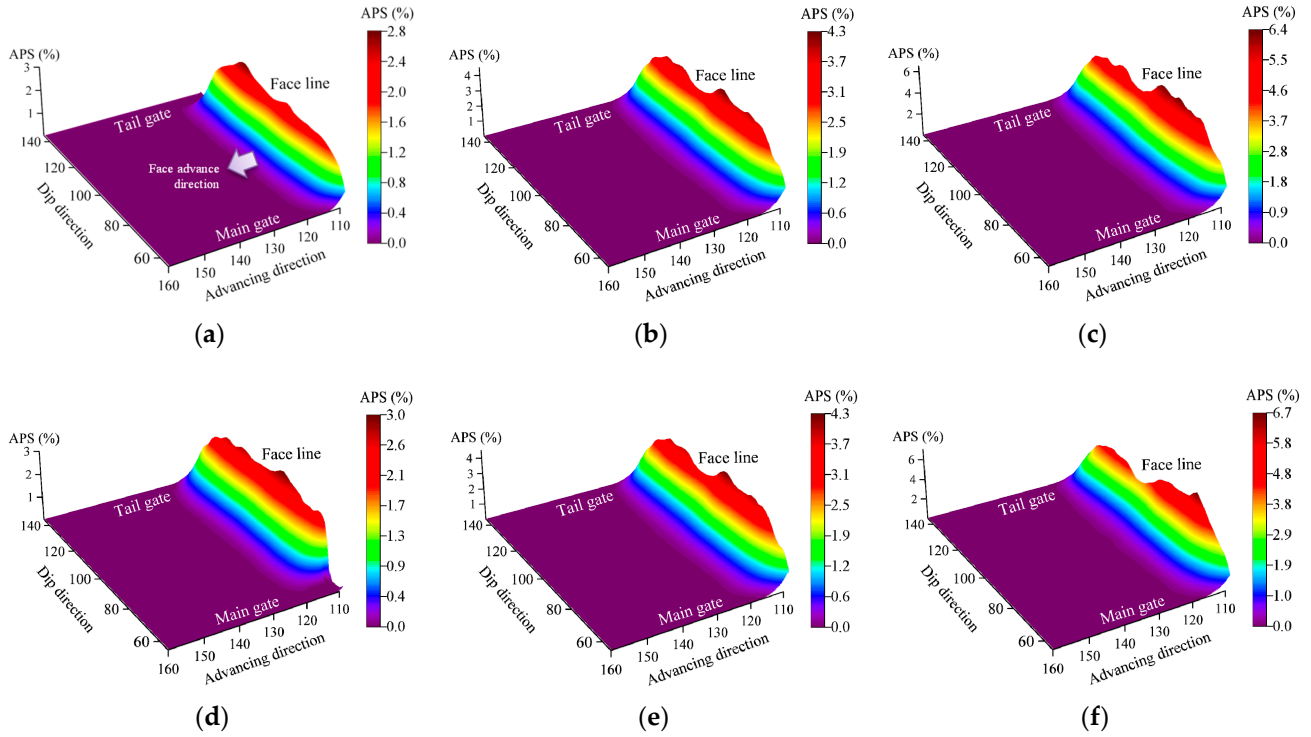

Figure 18. Influence of pre-existing fractures on APS of top-coal. (**a**) Model I; (**b**) Model II; (**c**) Model III; (**d**) Model IV; (**e**) Model V; (**f**) Model VI.

In accordance with the distribution of the failure zone, accumulation of the plastic strain is brought forward ahead of the longwall face due to the existence of hydraulic fractures. Plastic strain is accumulated within 12 m ahead of the longwall face in model I. The region is enlarged to 19 m in model III. In models IV, V, and VI, the plastic strain accumulation region expands from 13 m to 24 m with the growth of fracture length. At the rear of the face line, the APS of top-coal fluctuates dramatically along the panel width in the numerical models with hydraulic fractures. The maximum value increases from 2.4 to 6.0% as the number of fractures grows from 500 to 4000 and from 2.8 to 5.5% as the fracture length increases from 1.2 to 1.8 m. Thus, it can be concluded top-coal cavability is greatly improved with the growth in fracture intensity and fracture length due to hydraulic fracturing conducted in the thick coal seam. Thus, the top-coal cavability of the Dongzhouyao coal mine has been effectively improved due to the application of the hydraulic fracturing method. Accordingly, the top-coal recovery rate of the target longwall panel increases from about 75 to 83%, which results in great economic benefits.

5. Conclusions

In this study, top-coal failure mechanisms are analyzed, and the influence provided by hydraulic fracturing on top-coal failure behavior is discussed. Based on experimental and numerical results, the following conclusions are mainly reached.

(1) Maximum values of both major and minor principal stresses occur at the middle section of the panel width ahead of the longwall face. The minor principal stress, which dominates failure patterns of the top-coal, encompasses the transition from compressive to tensile state at the location nearly in front of the longwall face.

(2) Under the influence of the longwall mining, the top-coal first experiences shear failure in front of the longwall face and subsequently, undergoing tensile failure at the rear of the face line. Shear failure initiates at the lower level of the top-coal and propagates to the upper level. Top-coal cavability of the former is thus better than that of the latter.

(3) The APS of top-coal is taken as a quantitative indicator of the cavability in the present study. Along the panel width, the distribution of the APS and the principal stress displays similar characteristics. Their maximum values appear in the middle section consistently. In advancing direction, top-coal cavability is greatly enhanced with decreasing distance from the longwall face.

(4) Through hydraulic fracturing in thick coal seams, top-coal cavability is significantly enhanced. With increasing fracture intensity and fracture size, the failure zone expands significantly in front of the longwall face, and the APS of top-coal increases quickly. Besides, the spatial distribution of the APS transits from uniform to non-uniform type, which means the cavability varies greatly in the longwall face. Top-coal recovery rate increases from 75 to 83% in the target panel after the application of the hydraulic fracturing method.

Author Contributions: Conceptualization, Z.W.; methodology, Z.W. and Y.T.; software, H.G.; formal analysis, Y.T. and H.G.; resources, Y.T.; data curation, H.G.; writing—original draft preparation, Z.W. and Y.T.; supervision, Z.W. All authors have read and agreed to the published version of the manuscript.

Funding: This research was funded by the National Natural Science Foundation of China (51904304 and 51934008). The authors greatly appreciate their support.

Institutional Review Board Statement: Not applicable.

Informed Consent Statement: Not applicable.

Data Availability Statement: The Data are available upon request.

Conflicts of Interest: The authors declare no conflict of interest.

References

1. Wang, J.-C. *The Theory and Technique on the Thick Coal Seam Mining*; Metallurgical Industry Press: Beijing, China, 2009; ISBN 978-7-5024-5019-9.
2. Le, T.-D.; Oh, J.; Hebblewhite, B.; Zhang, C.; Mitra, R. A discontinuum modelling approach for investigation of longwall top coal caving mechanisms. *Int. J. Rock Mech. Min. Sci.* **2018**, *106*, 84–95. [CrossRef]
3. Xie, X.-Z.; Zhao, T.-L. Analysis on the top-coal caving structure of extra-thick hard coal seam with shallow depth in fully mechanized sublevel caving mining. *J. China Coal Soc.* **2016**, *41*, 359–366. (In Chinese)
4. Xie, H.-P.; Chen, Z.-H.; Wang, J.-C. Three-dimensional numerical analysis of deformation and failure during top-coal caving. *Int. J. Rock Mech. Min. Sci.* **1999**, *36*, 651–658. [CrossRef]
5. Yasitli, N.-E.; Unver, B. 3D numerical modeling of longwall mining with top-coal caving. *Int. J. Rock Mech. Min. Sci.* **2005**, *42*, 219–235. [CrossRef]
6. Khanal, M.; Adhikary, D.; Balusu, R. Evaluation of mine scale longwall top-coal caving parameters using continuum analysis. *Min. Sci. Technol.* **2011**, *21*, 787–796. [CrossRef]
7. Vakili, A.; Hebblewhite, B.-K. A new cavability assessment criterion for Longwall Top-coal Caving. *Int. J. Rock Mech. Min. Sci.* **2010**, *47*, 1317–1329. [CrossRef]
8. Alehossein, H.; Poulsen, B.-A. Stress analysis of longwall top-coal caving. *Int. J. Rock Mech. Min. Sci.* **2010**, *47*, 30–41. [CrossRef]
9. Wang, J.-C.; Bai, X.-J.; Wu, Z.-S. Study on top-coal broken size in sublevel caving face with hard coal seam. *J. China Coal Soc.* **2000**, *25*, 238–242. (In Chinese)

10. Xie, H.-P.; Chen, Z.-H.; Wang, J.-C. Fractal research on joints distribution in gateway. *J. China Coal Soc.* **1998**, *23*, 254–257. (In Chinese)
11. Jin, Z.-M.; Gong, P.-L.; Jin, W.-X. Fracturing characteristics of the top-coal. *Chin. J. Rock Mech. Eng.* **2002**, *21*, 70–82. (In Chinese)
12. Wang, K.; Zhang, B.; Kang, T.-H.; Chai, Z.-Y.; Yang, Y.-K. Physical simulation and engineering practice of cracks in coal mass matching with working face by fully-mechanized sublevel caving mining in shallow-buried coal seam. *Chin. J. Rock Mech. Eng.* **2013**, *38*, 2099–2105. (In Chinese)
13. Huang, B.-X.; Wang, Y.-Z.; Cao, S.-G. Cavability control by hydraulic fracturing for top-coal caving in hard thick coal seams. *Int. J. Rock Mech. Min. Sci.* **2015**, *74*, 45–57. [CrossRef]
14. Wang, P.; Jiang, L.; Jiang, J.; Zheng, P.; Li, W. Strata behaviors and rock burst–inducing mechanism under the coupling effect of a hard, thick stratum and a normal fault. *Int. J. Geomech.* **2018**, *18*, 04017135. [CrossRef]
15. Wang, J.-H. Development and prospect on fully mechanized top-coal caving in Chinese coal mines. *Int. J. Coal Sci. Technol.* **2014**, *1*, 253–260. [CrossRef]
16. Gao, H.-C.; Yang, S.-L.; Liu, X.-J. Hollow Inclusion in situ stress test method and engineering application. *Coal Eng.* **2015**, *47*, 83–85.
17. *FLAC3D (Fast Lagrangian Analysis of Continua in 3 Dismensions), Version 5.0*; ICG, Itasca Consulting Group, Inc.: Minneapolis, MN, USA, 2012.
18. Hoek, E.; Carranza-Torres, C.; Corkum, B. Hoek-Brown failure criterion-2002 edition. *Proc. NARMS Tac* **2002**, *1*, 267–273.
19. Wang, J.-C.; Wang, Z.-H.; Yang, S.-L. A coupled macro-and meso-mechanical model for heterogeneous coal. *Int. J. Rock Mech. Min. Sci.* **2017**, *94*, 64–81. [CrossRef]
20. Wang, J.-C.; Zhao, W.-B.; Zhao, P.-F.; Yang, S.-L.; An, J.-H. Research on the longwall top-coal caving mining technique in extremely inclined and soft thick coal seam. *J. China Coal Soc.* **2017**, *42*, 286–292. (In Chinese)
21. Zhang, G.-C.; He, F.-L.; Lai, Y.-H.; Jia, H.-G. Ground stability of an underground gateroad with 1 km burial depth: A case study from Xingdong coal mine, China. *J. Cent. South Univ.* **2018**, *25*, 1386–1398. [CrossRef]
22. Le, T.-D. Longwall Top Coal Caving Mechanism and Cavability Assessment. Ph.D. Thesis, University of New South Wales, Sydney, Australia, 2018.